

See discussions, stats, and author profiles for this publication at: <https://www.researchgate.net/publication/232907379>

# DFT Study on Anatase TiO<sub>2</sub> Nanowires: Structure and Electronic Properties As Functions of Size, Surface Termination, and Morphology

ARTICLE *in* THE JOURNAL OF PHYSICAL CHEMISTRY C · JULY 2010

Impact Factor: 4.77 · DOI: 10.1021/jp9090987

---

CITATIONS

25

READS

296

## 4 AUTHORS, INCLUDING:



Giovanni Cantele

Italian National Research Council

77 PUBLICATIONS 1,431 CITATIONS

[SEE PROFILE](#)



Fabio Trani

Italian National Research Council

44 PUBLICATIONS 757 CITATIONS

[SEE PROFILE](#)



Domenico Ninno

University of Naples Federico II

134 PUBLICATIONS 2,252 CITATIONS

[SEE PROFILE](#)

# DFT Study on Anatase TiO<sub>2</sub> Nanowires: Structure and Electronic Properties As Functions of Size, Surface Termination, and Morphology

Amilcare Iacomino,<sup>\*,†,‡,¶</sup> Giovanni Cantele,<sup>||</sup> Fabio Trani,<sup>§</sup> and Domenico Ninno<sup>||</sup>

*Dipartimento di Fisica “E. Amaldi”, Università degli Studi Roma Tre, Via della Vasca Navale 84, I-00146 Roma, Italy, CNISM, U. di R. Università degli Studi di Napoli “Federico II”, Dipartimento di Scienze Fisiche, Complesso Universitario Monte S. Angelo, Via Cintia, I-80126 Napoli, Italy, CNR-SPIN and Università degli Studi di Napoli “Federico II”, Dipartimento di Scienze Fisiche, Complesso Universitario Monte S. Angelo, Via Cintia, I-80126 Napoli, Italy, and Scuola Normale Superiore di Pisa, Piazza dei Cavalieri 7, 56126, Pisa, Italy*

Received: September 21, 2009; Revised Manuscript Received: May 7, 2010

We have performed first-principles calculations on anatase TiO<sub>2</sub> nanowires (NWs) to investigate the dependence of their structural and electronic properties on the size, the surface coverage, and the morphology. We have found that the overall crystallinity of the NWs increases on increasing the diameter size or equivalently upon surface coverage with simple water-derived adsorbates. The NWs grown along the [010] direction are found to be more ordered with respect to the NWs in the [001] direction of the same size, thus highlighting the dependence of the crystallinity on the choice of the morphology. The bare and hydrated NWs do show the band gap blue shift due to the size confinement, but deviations from an ideal trend with the size are found and ascribed to the morphology and the crystallinity. Through the analysis of the valence band maximum and conduction band minimum energies we found that the electrochemical potential variations of the TiO<sub>2</sub> NWs profit from the confined size, for example, by favoring the water splitting process. Moreover, the availability of internal channels for an efficient charge transport can be tuned by the surface coverage. The terminal hydroxyl groups of the hydrated NWs cannot be considered as deep hole traps since their related electronic states have binding energies in the same range of the NW oxygen states. The hydrogenated NWs grown along the [001] direction show occupied states at the bottom of the conduction bands, thus we expect that TiO<sub>2</sub> NWs can be used as efficient hydrogen sensors. Finally, the surface hydration leads to the most stable NWs among the considered surface configurations with formation energies that are even close to the bulk limit.

## Introduction

A main focus of the modern material research relies on the efficient tuning of the peculiar properties emerging at nanoscale to ultimately enhance specific processes of interest. A striking example in this field is represented by the huge efforts in controlling and tailoring the performance of titanium dioxide (TiO<sub>2</sub>) functional nanodevices, boosted by the relevant social and commercial rebounds of their applications. Nanostructured TiO<sub>2</sub> is employed in dye-sensitized solar cells, in gas sensing, in hydrogen production, in the disinfection of contaminated water and air, in the inactivation of bacteria, and in self-cleaning coatings.<sup>1–4</sup> The list is far from being completed given that TiO<sub>2</sub> is a wide band gap, cheap, and biocompatible n-type semiconductor able to photocatalyze several heterogeneous reactions. Actually, zero-dimensional (0D) TiO<sub>2</sub> nanoparticles (NCs) and one-dimensional (1D) nanowires (NWs) share the same benefits from having larger surface area, more active sites, and quantum confinement related properties that eventually lift the rates of their activity.<sup>4–11</sup> One-dimensional nanotubes, nanorods, and NWs are sometimes polycrystalline assemblies of NCs,<sup>12–16</sup> hence the elementary physical properties can overlap. The main

feature that can distinguish 1D TiO<sub>2</sub> nanostructures from their 0D counterpart is a better ability to transport (photo)generated charges away from possible (recombination) reaction sites, thus revealing the heavy attention that they are receiving for applications in photovoltaic cells, sensors, electrodes, and optoelectronics.<sup>17–22</sup>

Theoretical investigations may fill the gap through the atomistic modeling of TiO<sub>2</sub> nanostructures by proposing the fundamental understanding of the physical properties behind the observed mechanisms at the nanoscale. Despite the example of the well-characterized 1D nanomaterials like silicon and carbon, a very scarce literature is directly focused on the study of TiO<sub>2</sub> 1D nanostructures up to now. Enyashin et al.<sup>23</sup> proposed a model describing the stability of (anatase and dehydrogenized lepidocrocite-based) nanotubes, nanorolls, and nanostrips of TiO<sub>2</sub> as a function of the radius, by using a density-functional-based tight-binding method. They also reported the convergence of the band gap to the bulk value for radii of about 25 Å but without considering the effect of the surface interactions with environment species. Allen<sup>24</sup> speculated on the geometric construction of 1D formula units that can take advantage of the translational and rotational symmetries to design dipole-free, charge-neutral, and minimal surface polarized rutile and anatase NWs. Alvarez-Ramirez et al.<sup>25</sup> performed ab initio molecular dynamics calculations to determine the transformation mechanism of anatase wires in titanate-type structures, highlighting the important factor played by the adatoms that mimic the environment interactions. Zhang et al.<sup>26</sup> tested the stability

\* To whom correspondence should be addressed: E-mail: amilcareiacomino@gmail.com.

† Università degli Studi Roma Tre.

‡ CNISM.

|| CNR-SPIN and Università degli Studi di Napoli “Federico II”.

§ Scuola Normale Superiore di Pisa.

¶ Current address: Universidad del País Vasco, San Sebastián, Spain.

of the two thinnest  $\text{TiO}_2$  NWs assembled from dimeric  $\text{Ti}_2\text{O}_4$  molecules as basic building blocks within the density functional theory (DFT) approach. At last, Meng et al.<sup>27</sup> have recently shown the ultrafast electron injection from a dye molecule to anatase NWs by means of time-dependent DFT.

The aim of this work is to investigate the dependence of the structural, electronic, and stability properties of anatase  $\text{TiO}_2$  NWs as functions of the surface coverage, of the diameter size, and of the morphology within the framework of first-principles DFT calculations. It is experimentally possible to synthesize  $\text{TiO}_2$  NWs starting from NC as building blocks with one possible elongation of the chain being the [001] direction.<sup>28–30</sup> We took advantage of our previous study on  $\text{TiO}_2$  NCs<sup>31</sup> to construct the bare NW presented in this work, which is cut by the (100) and (010) planes and periodic along the [001] axis. We then defined an analogous NW with a larger diameter to verify the trends in size of the calculated properties. Both NWs were then covered with simple water-derived species to simulate two different environments in which they could be synthesized or catalyze reactions. A second type of NW periodic in the [010] direction and with lateral surfaces derived from cutting by the (001) and (101) planes was compared to the previous ones to find peculiarities related to the geometric arrangements. The following points summarize the main findings that are going to be unraveled in the following:

- Terminal atoms of the surface are directly involved in the photocatalytic processes, since both charge transfers and bonds occur at the interface. The structural organization of these atoms is different with respect to the ideal bulk configuration because of the truncation of the crystal field. This difference sums to the specific properties of each surface thus determining the final behavior in terms of chemical stability and catalytic efficiency. The presence of edges, corners, and different local arrangements in nanomaterials can affect the overall features more significantly than in the macroscopic samples. Nevertheless, to the best of our knowledge there are no available data on the atomic displacements and reconstructions at the  $\text{TiO}_2$  NWs surface. It should also be considered that the smallest diameters (1–6 nm)<sup>5,32–38</sup> of 1D nanostructures are in the same range of the 0D NCs for which surface distortions are reported.<sup>39–42</sup> Through total energy optimizations, we show the effects of the surface reconstruction on the whole crystallinity of the NWs in the section devoted to the structural properties.

- Scaling the dimension down to the nanometer range should lead to quantum size effects, as the band gap blue shift. It could contribute to improve the charge transfer between the NW and the reactive species if a proper line-up of the valence band maximum (VBM) for holes or conduction band minimum (CBM) for electrons with respect to the redox couple potentials is satisfied. The anatase  $\text{TiO}_2$  crystal is an indirect semiconductor and the onset radius of 0D NCs at which the blue shift is detectable, as well as the nature of the transition, has been a matter of debate.<sup>43,44</sup> The exciton radius is reported in the range 0.35–1.9 nm<sup>43,45</sup> while the effective mass for hole and electron is not unambiguously determined,<sup>43</sup> such that even the effective mass approximation has been considered arguable for small  $\text{TiO}_2$  NCs.<sup>44</sup> It follows that some NCs are blue shifted in the range 1–10 nm,<sup>46–49</sup> while others show the bulk band gap down to 1.5 nm.<sup>43,44</sup> The same controversy stands for 1D NWs, whose diameter acts as the confinement direction. However, a better crystallinity should preserve a more ideal behavior against the effects of the preparation methods and surface environment, hence blue shifts of 0.1–0.5 eV are reported for  $\text{TiO}_2$  1D nanostructures in the diameter range of 2–9 nm.<sup>9,35,50,51</sup> In this

work, we discuss the electronic properties of the NWs through calculations of the density of states (DOS) and of the charge density distribution of the states. A line-up of the bands energies of the NWs will elucidate the effect of the size, of the surface configuration, and of the morphology on the NW electrochemical potential, which can be ultimately related to the photocatalytic performances.

- Nanostructured  $\text{TiO}_2$  is widely investigated for large scale hydrogen production from water splitting and as hydrogen sensor.<sup>10,52–56</sup> These relevant outcomes need a systematic understanding of the interaction of the water constituents with the surface of  $\text{TiO}_2$  NWs. Among different synthesis techniques, solvothermal and hydrothermal methods can lead to NWs with water-capped surface, mainly because of the presence of hydroxylated terminations.<sup>51,57</sup> Several photocatalytic reactions of  $\text{TiO}_2$  nanostructures are performed in aqueous media, hence a considerable number of hydroxyl groups adsorbed on the surface can play an important role in the activity of the nanostructures.<sup>35</sup> The presence of a hydration sphere is usually observed to surround  $\text{TiO}_2$  NCs with a dissociative adsorption of the first water layer to prevail due to the ability to fill surface vacancies in the synthesis process.<sup>58,59</sup> We thus considered the coverage of the bare NWs with simple water derived adsorbates, modeling the surface configuration in the presence of hydrogen and hydration. We discuss in the last section the deep influence that the surface functionalization plays in determining the overall structural, electronic, and stability properties of these 1D NWs.

## Methodology

**Computational Details.** All ab initio calculations are performed within the DFT framework implemented in the Quantum-ESPRESSO package<sup>60</sup> based on plane waves and pseudopotentials. We used the generalized gradient approximation (GGA) parametrized with the Perdew–Wang (PW91) exchange-correlation functional<sup>61</sup> and Vanderbilt ultrasoft pseudopotentials.<sup>62</sup> The plane-wave basis set was chosen with a kinetic energy cutoff of 30 Ry for the wave functions and 180 Ry for the total charge. The Brillouin zone for the band structure calculation was sampled by a  $8 \times 1 \times 1$  Monkhorst-Pack  $k$ -point grid,<sup>63</sup> if considering the  $x$ -axis as the direction of periodicity for the NWs. The NWs geometry is optimized with the direct energy minimization technique of Broyden–Fletcher–Goldfarb–Shanno,<sup>64</sup> based on the calculation of the Hellman–Feynman forces. The optimization is stopped when each Cartesian component of the force acting on each atom is less than 0.026 eV/Å. All the presented properties are referred to the optimized systems. A vacuum gap of at least 10 Å separates each NW from its periodic replica in neighbor supercells to avoid spurious interactions. A satisfactory convergence of the calculated properties with respect to the above parameters has been carefully checked. The structural optimization of the tetragonal three-dimensional anatase crystal gave lattice constants  $a = 3.809$  Å and  $c = 9.604$  Å, whereas the internal dimensionless parameter is  $u = 0.208$ . All three numbers compare well to the experimental values (at 15 K) 3.782 Å, 9.502 Å, and 0.208 respectively.<sup>65</sup> The starting geometry of the  $\text{TiO}_2$  NWs is defined with atoms at the ideal crystal positions. The atomic positions were then randomized by 1% to break symmetries and thus ensuring an unconstrained and more physical relaxation. To check the dependence of our results on the exchange and correlation functional and spin polarization, we performed all the calculations for the whole set of thinnest NWs with a LDA exchange and correlation functional and also including the spin polarization. In both

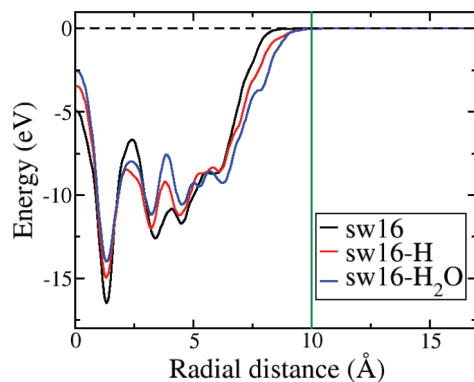


**Figure 1.** Plot of the averaged electrostatic potential on cylinders coaxial with the NW. The green vertical line highlights the distance from the axis where the averaged potential approaches the flat value. The three curves refer to a bare NW (black curve) and its hydrogenated (red) and hydrated (blue) surface counterparts.

cases, no significant variations of the calculated properties have been found. For example, the energy gap changes are less than 0.05 eV.

To compare the Kohn–Sham levels coming from the different calculations based on our plane-wave approach, we needed a reliable procedure to set a common zero energy reference for the bands energy alignment. This bands energy alignment of all the NWs is achieved by calculation of a mean electrostatic potential as function of the distance from the NW axis. At a fixed distance, this mean electrostatic potential is the average on the surface of a cylinder coaxial to the NW. The flat value of the averaged electrostatic potential in the vacuum region is defined as the vacuum level and shifted to 0 eV (reference energy). All the single state eigenvalues are accordingly shifted such that the energy of the VBM matches the ionization potential. In Figure 1, we report the application of this procedure to a set of NWs that we have studied in this work, where it is possible to see the trend of the averaged potential to a flat value as the distance from the NW axis increases. In the section dealing with the electronic properties, we will show that this procedure gives reliable results which can be directly connected to the experiments.

**NWs Definition.** In Figure 2, we show that the smallest bare and stoichiometric NW (labeled sw9) studied in this work is made up of 27 atoms in the unit cell with chemical formula (TiO<sub>2</sub>)<sub>9</sub>. This NW directly follows from the model proposed by Liu and Yang in an experimental effort to synthesize angstrom-scale titania NWs, which are the thinnest anatase TiO<sub>2</sub> NWs assembled to our knowledge.<sup>32</sup> The sw9 NW elongates in the [001] direction, which is a common growth direction of anatase 1D nanostructures due to the anisotropy of the TiO<sub>2</sub> crystal and to the different reactivity of the (001) surface with functionalizing species in the synthesis process.<sup>1,28</sup> A first kind of surface coverage is achieved by bonds with single hydrogen atoms (H) of the undercoordinated atoms of the surface.<sup>31</sup> This NW (sw9-H) has chemical formula in the unit cell (TiO<sub>2</sub>)<sub>9</sub> H<sub>20</sub>. The hydrogenation coverage is meant to model the NWs in extreme acidic environments or the exposure of naked NWs to a H<sub>2</sub> atmosphere.<sup>55,70</sup> The second surface coverage is obtained bonding with H atoms the undercoordinated oxygens of sw9 and with OH groups the undercoordinated Ti, thus closing their octahedral coordination. The resulting NW (sw9-H<sub>2</sub>O) has chemical formula (TiO<sub>2</sub>)<sub>9</sub> (H<sub>2</sub>O)<sub>12</sub> in the unit cell. This hydration coverage is meant to model a moderate pH environment in which a complete dissociative adsorption of water takes place.

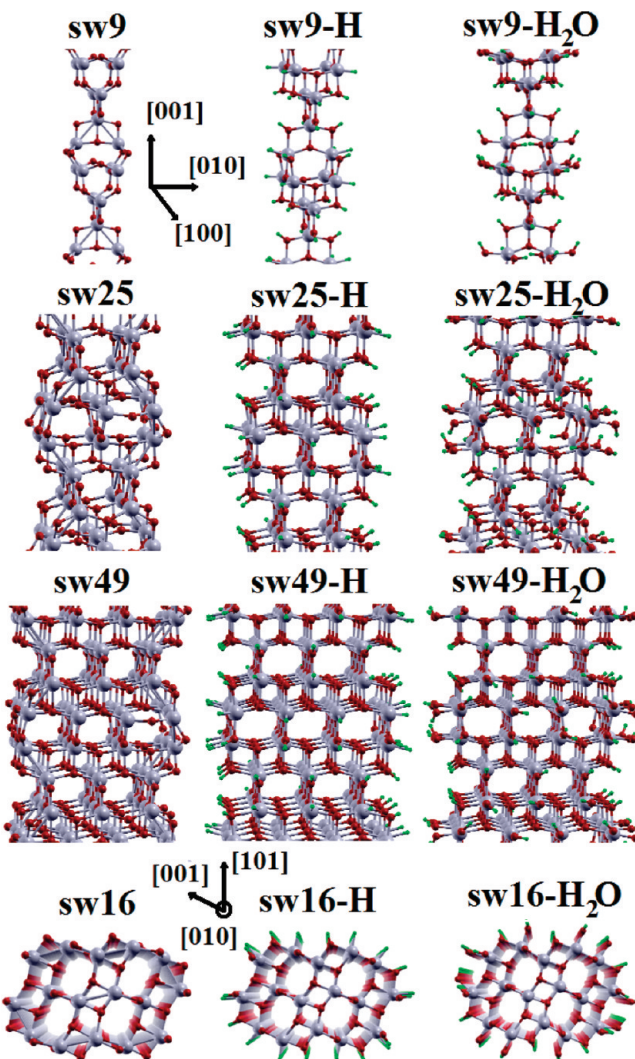


**Figure 2.** Optimized structures of the stoichiometric NWs. Ti atoms are in gray, O atoms are in red, and H atoms are in green. The first type NWs are elongated in the [001] direction whereas the second type NWs (bottom row) are elongated in the [010] direction. Bare NWs are in the left column, hydrogenated NWs in the central column, and hydrated NWs in the right column with their respective label reported on top.

The OH groups can also model the same stabilizing role of the functionalizing species employed in the NW production.<sup>28</sup>

The second bare and stoichiometric NW (sw25) studied in this work is made up of 75 atoms in the unit cell with chemical formula (TiO<sub>2</sub>)<sub>25</sub>. Its morphology derives by the connection of single NCs, which we studied in a previous work,<sup>31</sup> to form a chain in the [001] direction. The lateral surfaces expose the (100) and (010) planes, which occasionally occur in nanostructured TiO<sub>2</sub>.<sup>30,35,66–69</sup> Ti atoms are at least 4-fold coordinated while O atoms are at least 2-fold coordinated. As for sw9, we considered both hydrogenation and hydration. The hydrogenated NW (sw25-H) has chemical formula in the unit cell (TiO<sub>2</sub>)<sub>25</sub> H<sub>36</sub>. The hydrated NW (sw25-H<sub>2</sub>O) has chemical formula (TiO<sub>2</sub>)<sub>25</sub> (H<sub>2</sub>O)<sub>20</sub> in the unit cell.

The third bare and stoichiometric NW (sw49) of this morphological set is made up of 147 atoms in the unit cell with chemical formula (TiO<sub>2</sub>)<sub>49</sub>. It retains the same axial direction and exposed surfaces as sw25 but with a longer diameter. In this way, we can span the range of 1 nm size to give a trend in dimension of the calculated properties. This bare NW is also considered in its covered configurations, the hydrogenated

sw49-H and the hydrated sw49-H<sub>2</sub>O with chemical formula (TiO<sub>2</sub>)<sub>25</sub>H<sub>52</sub> and (TiO<sub>2</sub>)<sub>25</sub>(H<sub>2</sub>O)<sub>28</sub>, respectively. At last, we calculated a naked NW (sw81) with the same morphology and a diameter of 1.524 nm (figure not shown). For all the NWs of this morphology, the cell dimension along the periodic *x* axis is fixed at the optimized value of 9.604 Å.

The fourth bare and stoichiometric NW (sw16) contains 48 atoms in the unit cell with chemical formula (TiO<sub>2</sub>)<sub>16</sub>. It is periodic in the [010] direction and the lateral surfaces are derived by cutting with (101) and (001) planes. In this case, Ti atoms are at least 5-fold coordinated. This second type of NW is used to identify properties related to morphological aspects as the growth direction and the exposed surfaces. The hydrogenated form (sw16-H) has chemical formula (TiO<sub>2</sub>)<sub>16</sub>H<sub>20</sub> while for the hydrated NW (sw16-H<sub>2</sub>O) it is (TiO<sub>2</sub>)<sub>16</sub>(H<sub>2</sub>O)<sub>10</sub> in the unit cell. For all the NWs of this second morphology, the cell dimension along the periodic *x* axis is fixed at the optimized value of 3.809 Å.

## Results and Discussion

**Structural Properties.** The microscopic knowledge of the local structural features of TiO<sub>2</sub> nanostructures is a critical issue for the understanding of the properties that emerge at the nanoscale. The fundamental question to be addressed is the relevance of the profusion of specific geometric and local arrangements on the overall performance and activity of the nanosamples. The theoretical modeling is thus a necessary tool to push the microscopic investigation of TiO<sub>2</sub> NWs on a purely atomistic scale, where the current available experimental techniques may encounter challenging tasks to overcome. In this section, we show that the structural properties of the NWs depend on the diameter size, on the morphology, and on the surface termination. These are factors that can deeply influence the behavior of the nanosamples in real applications and must be taken into account when designing new TiO<sub>2</sub> nanomaterials.

**Section Area Variations.** We have estimated the transversal variations of the area of a NW section by comparing the section area of an optimized NW with that of the NW with the atoms at the bulk positions. The section area of a given NW is computed as  $A = \Delta d_x \Delta d_y$ , where  $\Delta d_i$  is the diameter along the *i* axis. Keeping the crystallographic notation the axes are {*x* = [010], *y* = [100]} for the first type NWs periodic along the [001] direction and {*x* = [100], *y* = [001]} for the second type NWs periodic along the [010] direction, while  $\Delta d_i$  is computed as the distance between the outermost Ti atoms along the *i* direction.

From Table 1 it can be seen that the section of all the bare NWs is contracted with respect to the ideal bulk value, whereas the surface coverage always leads to the expansion of the section. Thus, the presence of adsorbates at the surface can compensate and eventually invert the own trend of TiO<sub>2</sub> NWs to contract inward. This first result must be considered when measuring the lattice parameters variations in real NWs as they always undergo surface interactions either in the synthesis process, either due to functionalizations for specific applications, or in the final working environment. It can also explain the contrasting experimental results on the lattice variations with the size observed for TiO<sub>2</sub> NCs synthesized with different techniques.<sup>71</sup>

The bare NWs section is more and more contracted with respect to the ideal (unrelaxed) size as the diameter decreases, which is actually found for TiO<sub>2</sub> nanoparticles larger than 10 nm.<sup>72</sup> Hence naked TiO<sub>2</sub> NWs are expected to contract with the size reduction. At variance with this trend, water-covered

**TABLE 1: Diameters ( $\Delta d_x$ ,  $\Delta d_y$ ), Section Area ( $A = \Delta d_x \Delta d_y$ ), and Section Area Variations ( $\Delta A = (A - A_0)/A_0$ ,  $A_0$  Being the Section Area of the NW with the Atoms in the Ideal Bulk Positions) of the NWs<sup>a</sup>**

system	$\Delta d_x$ (Å)	$\Delta d_y$ (Å)	$A$ (Å <sup>2</sup> )	$\Delta A$ (%)
ideal	3.809	3.809	14.51	
sw9	3.167	3.566	11.29	-22.2
sw9-H	3.859	3.752	14.48	-0.3
sw9-H <sub>2</sub> O	4.016	4.170	16.75	+15.4
ideal	7.618	7.618	58.03	
sw25	7.180	7.181	51.56	-11.1
sw25-H	7.788	7.819	60.89	+4.9
sw25-H <sub>2</sub> O	7.884	7.712	60.85	+4.8
ideal	9.522	12.005	114.31	
sw16	9.266	11.717	108.57	-5.0
sw16-H	9.711	12.340	119.83	+4.8
sw16-H <sub>2</sub> O	9.789	12.084	118.29	+3.5
ideal	11.427	11.427	130.58	
sw49	11.053	11.012	121.71	-6.8
sw49-H	11.618	11.620	135.00	+3.4
sw49-H <sub>2</sub> O	11.685	11.681	136.49	+4.5
ideal	15.236	15.236	232.14	
sw81	14.923	14.901	222.37	-4.2

<sup>a</sup>  $\Delta d_x$  and  $\Delta d_y$  are calculated as the distance along the respective axes (*x*, *y*) between the two outermost Ti atoms (keeping the crystallographic notation *x* = [100], *y* = [010] for the first type NWs and *x* = [100], *y* = [001] for the second type NWs).

NWs undergo an increasing expansion with decreasing size. This second result is in agreement with the volume trend of the TiO<sub>2</sub> nanoparticles below the 10 nm size assumed from experiments.<sup>72</sup> Thus we can explain the overall trend upon size reduction in terms of competing phenomena. On one hand, anatase TiO<sub>2</sub> NWs have their own tendency to contract but, on the other hand, the presence of surface adsorbates induce the opposite effect. Thus, when the size is shorter than 10 nm the surface dislocations prevail and a clear contraction is detected. At the end, the second type NWs grown along the [010] direction (sw16 series in Table 1) show variations in the trend of the section area with respect to the first type NW of comparable size. Both the bare sw16 and the hydrated sw16-H<sub>2</sub>O have smaller variations than the first type NWs. Hence by changing the exposed surfaces and the growth direction it is possible to tune the NW crystallinity against variations of the size and of the surface configuration.

**Variations of the Atomic Distances.** We analyzed the bond lengths and the distances between atoms in the NWs to have a picture of the deviation from an ideal perfect crystallinity, which is unavoidable in the real nanosamples. We show here the result of this study through plots of the distribution of the distance between atomic pairs.

All the NWs show distortions (with respect to the ideal, bulk positions) in the geometry of the bonds as well as of the long-range distances between the atoms. Hence a change of the coordination numbers of the bulk atomic shells is revealed by the distribution of distances around the bulk ideal values, as shown in Figure 3a for the case of the Ti–O distances in the sw49 NW series. The surface coverage is always found to preserve a better structural order with respect to the bare NWs. This result can be seen by the smaller dispersion of the distances around the bulk values that results in the long-range order of the covered NWs. Thus the first result clearly points out that the surface termination with proper adsorbates is determinant to synthesize well-ordered and crystalline NWs with diameters in the (sub)nanometer range, as obtained in ref 32. The largest atomic displacements are found for the NWs terminal atoms,

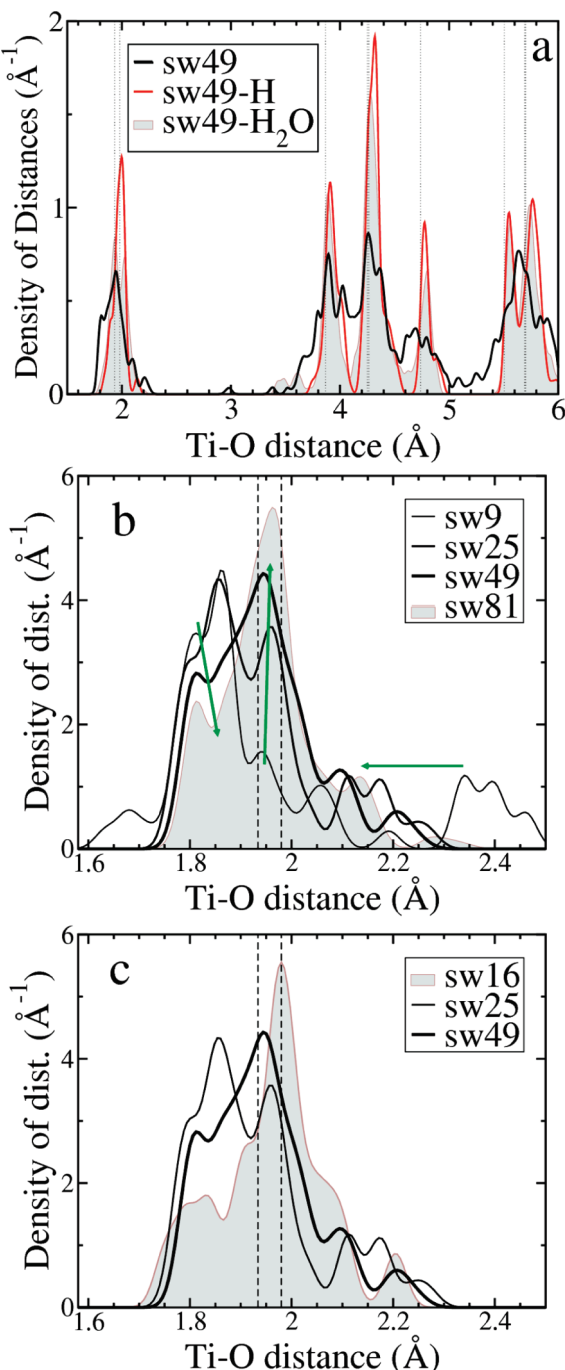


**Figure 3.** Distribution of the atomic distances density for (a) the sw49 series of NWs, (b) the first type bare NWs, and (c) the bare second type NW sw16 and the bare first type NWs (sw25 and sw49) of comparable size. Vertical dashed lines correspond to the bulk distances, while the green arrows in (b) highlight the effect of the size increase on the relevant peaks. A fictitious Gaussian broadening ( $\sigma = 0.03 \text{ \AA}$ ) is attributed to each distance to give a clearer picture. The complete set of graphs is provided in the Supporting Information, Figures 1–3.

upon covering the surface. In fact, the adsorbates induce an outward shift of the NW atoms that are instead contracted in the bare NWs. Furthermore, the inner atoms of the covered NWs faithfully reproduce the bulklike geometry. Hence, we agree with the very recent suggestion that for anatase nanocrystals a core–shell picture of the structural organization can be inferred:<sup>72</sup> internal atoms preserve the (ideal) anatase crystal arrangement whereas a surface shell of atoms is more or less distorted

according to the local surface environment and to the availability of adsorbates.

The overall crystallinity of the NWs also depends on the diameter size. On increasing the size in the first type NWs the octahedral coordination of the titanium atoms, the geometry of the bonds, and the atomic distances are closer and closer to the corresponding bulk values. In Figure 3b, we summarize this trend focusing on the short-range order of the Ti–O bonds of the bare NWs. As shown by the green arrows, the main peaks of the distance distribution shift to the bulk bond lengths as the size of the NW increases. In fact, the peaks outside the range of the bulk values (vertical dashed lines) loose their intensity or shift to the bulk values whereas the peak at the bulk values increases its intensity. Hence the long-range effects of the local surface disorder can be diminished by increasing the size, yet they cannot be eliminated.

As a last result, we mention that the morphology of the NWs also contributes to change the effects of the size on the structural distortions. In fact, we found that the second type NWs grown along the [010] direction have a better crystalline order than the first type NW grown along the [001] direction of comparable size, namely the sw25 and sw49 series. The result also holds for the surface covered NWs, but to give an easy picture of this dependence we show in Figure 3c the Ti–O distribution of distances in the bond lengths range of the bare NWs. The second type NW sw16 shows a structural order that is close to the largest studied NW sw81 with a diameter of 15 Å. That is, for a fixed diameter size different growing orientations do show different degrees of crystallinity. We conclude that the choice of the exposed crystallographic surfaces and of the growing direction can be factors to be taken under consideration when the crystallinity of the nanosamples is a crucial parameter for the applications of these TiO<sub>2</sub> NWs. Equally, if the size of a NW is fixed, the choice of an appropriate adsorbate can have the same effect of preserving a better crystallinity with respect to a bare free-standing NW.

**Electronic Properties. Effects of the Size Reduction.** Many aspects concerning the size reduction in TiO<sub>2</sub> nanostructures are still object of debate. Unraveling such aspects is crucial to employ such materials in the future generation of optical and electronic devices. First of all, we mention the increase of the band gap in the quantum confinement regime due to the shrinking of the material below the exciton radius ( $r_{\text{ex}}$ ). Experiments on TiO<sub>2</sub> nanostructures do not always agree in detecting the band gap blue shift upon size reduction.<sup>43</sup> This also applies to the 1D NWs, as they can be grown as agglomerates of NCs.

To detect the blue shift of the band gap it is sufficient that the material size in one direction is of the order of  $r_{\text{ex}}$ . The size of the TiO<sub>2</sub>  $r_{\text{ex}}$  is not unambiguously determined and it is reported in the range 0.35–1.9 nm.<sup>43,45</sup> Our model systems fit in this range as their size goes from 3.81 Å for the thinnest sw9 NW to 15.24 Å for the largest sw81 NW. The anatase crystal is an indirect-gap semiconductor with the first transition ( $\sim X \rightarrow \Gamma$ ) at 3.2 eV. Our calculation on the bulk crystal gives a band gap of 2.08 eV that well compares with other theoretical calculations based on the DFT,<sup>73–75</sup> but it is clearly an underestimation of the real band gap (this is an usual shortcoming of the DFT). We expect that this underestimation does not affect our results since it should be independent of the dimensionality of the system. As reported in Table 2, the bare NWs of the first type, elongated in the [001] direction, show a band gap blue shift with respect to the bulk value that goes from 0.18 eV for the largest sw81 to 0.67 eV for the thinnest

**TABLE 2: Valence Band Maximum Energies (VBM) Scaled with Respect to the Vacuum and to the SHE Reference<sup>a</sup>**

system	VBM (eV) <sup>b</sup>		
	vs vacuum	vs SHE	$\Delta E_g$ (eV)
bulk <sup>c</sup>	-7.13	+2.69	
thin film <sup>d</sup>	-6.94	+2.50	
sw9	-7.25	+2.81	0.67
sw25	-7.21	+2.77	0.59
sw49	-7.26	+2.82	0.34
sw81	-7.18	+2.74	0.18
sw16	-7.01	+2.57	0.06
sw9-H <sub>2</sub> O	-6.77	+2.33	1.22
sw25-H <sub>2</sub> O	-6.94	+2.50	0.65
sw49-H <sub>2</sub> O	-6.72	+2.28	0.45
sw16-H <sub>2</sub> O	-6.54	+2.10	0.53
sw9-H	-7.56	+3.12	metal
sw25-H	-7.55	+3.11	metal
sw49-H	-7.37	+2.93	metal
sw16-H	-7.49	+3.05	-0.61

<sup>a</sup>  $\Delta E_g$  is the band gap difference with respect to the bulk value.  
<sup>b</sup> VBM energies of hydrogenated NWs correspond to the top O 2p states. <sup>c</sup> From ref 81. <sup>d</sup> From ref 77.

sw9. This is a clear indication that the size reduction affects the band gap blue shift. As expected on a general ground, the amount of blue shift increases with the size reduction and the fact that the largest sw81 presents a 0.18 eV blue shift leads us to conclude that the TiO<sub>2</sub>  $r_{\text{ex}}$  is at least of 1.5 nm. Interestingly, the second type NW sw16 shows a small band gap variation with respect to the bulk crystal ( $\Delta E_g = 0.06$  eV) even if its diameter is comprised between the sw25 and the sw49 ones. The degree of structural distortion is not so different between the two types of bare NWs to account for such a deviation, thus we ascribe the substantially unchanged band gap of sw16 to a morphological origin. The second type NWs expose the (101) and (001) surfaces that are typically more stable in the most common conditions. TiO<sub>2</sub> nanostructures with these surfaces as the major fraction of the surface facets can retain bulklike properties hence hindering the effect of the size reduction by making difficult the detection of the band gap blue shift down to the smallest samples. This result unravels a possible explanation of the disagreement of the blue shift measurements, in that a dependence of the quantum confinement effect on the morphology of the nanostructure comes out.

The effect of the structural distortion on the band gap becomes visible by considering the more ordered hydrated NWs. As reported in Table 2, all hydrated NWs show a higher blue shift with respect to their bare configuration. Moreover, the band gap shift of the (second type) sw16 NW falls between the sw25 and sw49 ones, as it should be for an ideal trend of the blue shift with the size. As discussed in the previous section, hydrated NWs have the highest crystallinity, which means that as the size of TiO<sub>2</sub> nanostructures decreases the effects of the local bonds geometry, surface reconstruction, and structural order become more and more relevant in determining the final electronic properties. This suggests that particular attention must be paid in synthesizing well-ordered TiO<sub>2</sub> NWs to detect quantum confinement phenomena.

The electronic properties of hydrogenated NWs deviate from the other surface configurations because in-gap states appear. Both types of NWs show occupied bands above the VBM energy that correspond to surface defect levels localized on the Ti–H bonds. The second type NW sw16-H, elongated in the [010] direction, preserves its semiconductive band gap but the first type hydrogenated NWs have occupied bands at the

bottom of the CBM energy with the band gap closing to less than 60 meV. Hence, a metallic behavior is expected for this morphology of TiO<sub>2</sub> NW that once again stresses the importance of the geometric design of this nanostructured material. Interestingly, experiments on TiO<sub>2</sub> NCs reveal the possibility of H lattice diffusion to produce free conduction band electrons from infrared excitation.<sup>76</sup> Moreover, conductance enhancement of order of magnitudes has been detected in TiO<sub>2</sub> nanotubes upon exposure to hydrogen gas.<sup>54</sup> We will debate in detail this topic in the section dealing with the hydrogen sensing ability of the NWs.

The second issue discussed in this section is related to the efficiency of TiO<sub>2</sub> NWs to support photocatalytic reactions and the charge transport to external circuits (for photosensing and solar cells). Both mechanisms are linked to the nature of the charge density distribution of the states involved in the transfer of charges. In fact, the probability of the charge transfer increases with the overlap between the donor/acceptor wave functions of the NW and the reactant. To support the transport of photoelectrons throughout the external circuit it is also necessary that conduction band channels flow inside the NW to lengthen the lifetime of charges by avoiding recombination centers, that is, structural distortions, defects, and charge traps that are mainly located at the surface.

From the analysis of the projection of the density of states on the atomic orbitals, we found that both highest valence bands and lowest conduction bands involve atoms located at the surface, particularly for the bare NWs (see Figure 4). This means that the size reduction effectively turns in favor of higher photocatalytic performances. Interestingly hydration of the surface is found to produce states with a spatial distribution of the density that is higher inside the NWs structure than that belonging to the states in same energy region of the bare NWs, see as example the effect of H<sub>2</sub>O on the LUMO state of the sw25 NW in Figure 4.

This effect sums to a better crystallinity of the hydrated NWs thus entailing the possibility to design surface configurations that optimize the availability of internal channels for the transport of electrons. To this purpose, it is noteworthy that the water-induced inward shift of the charge density is not appreciable only for the conduction bands of the second type NW sw16, hence it is important to select appropriate adsorbates according to the morphology of the NWs. The highest valence bands states with O 2p orbital character are delocalized on the surface thus being readily available for the charge transfer with adsorbates. On the other hand, the lowest conduction bands states with Ti 3d orbital character are delocalized inside the NWs with tails on the surface atoms. This ensures both the possibilities for photoelectrons to be exchanged with the adsorbates and move along the NW axis. In conclusion, the NWs are found to profit from the size confinement since the charge density of their states in the band gap region involves atoms at the surface, where the most of photocatalytic reactions takes place. Furthermore the interaction with water induces variations in the wire field that end up with the modulation of the spatial distribution of the NWs wave functions, thus proving the possibility to tune the electronic properties by specific surface configuration. The adsorbates can be functional to preserve a better crystallinity of the thinnest NWs on one hand and to confer peculiar properties to the electronic channels on the other.

**Bands Line-Up.** In this section, we discuss the distribution of electronic levels in the “bulk” band gap region since they are important in determining the relationship between the redox potentials of the nanostructured TiO<sub>2</sub> and the reactive couple

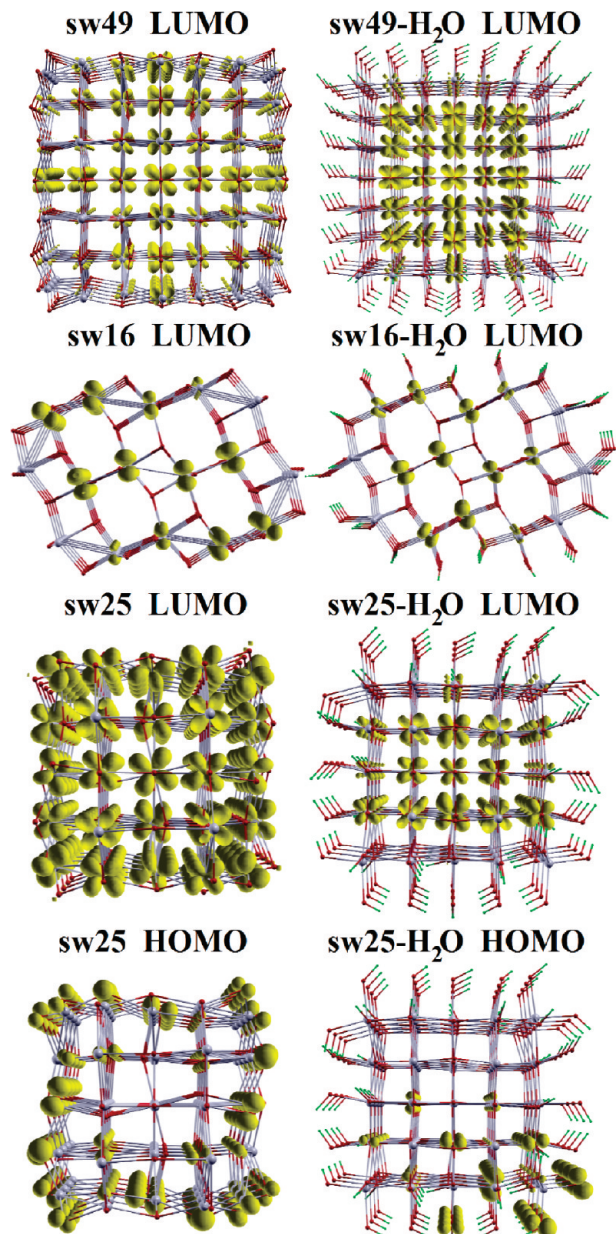


**Figure 4.** Charge density contour plots (10% of the maximum value) for some relevant electronic states lying in the gap region. The charge densities are localized on the surface for the bare NWs. On the other hand, the states in the gap region of surface covered NWs show charge densities with higher intensities inside the NWs than isoenergetic states of the bare NWs. This effect is not appreciable only for the lowest energy conduction bands of the second type NW sw16.

adsorbed at the surface. This relationship establishes the direction of a reaction when the two reactants are placed together. A striking example is the evolution of H<sub>2</sub> and O<sub>2</sub> in the water splitting process for which nanostructured TiO<sub>2</sub> is willing to be used. By illuminating TiO<sub>2</sub> nanostructures, the photogenerated holes (h<sup>+</sup>) can oxidize water molecules to produce hydroxyl radicals and protons, while photogenerated electrons (e<sup>-</sup>) flow to the photocathod and produce molecular hydrogen by reducing the protons. The former oxidation process takes place if the TiO<sub>2</sub> VBM energy is more positive than the water redox potential on an electrochemical scale (i.e., vs SHE, the standard hydrogen electrode). The latter reduction process is allowed if the TiO<sub>2</sub> CBM energy is more negative than the hydrogen redox potential. We calculated the line-up of the bands energies of our model systems with respect to the vacuum

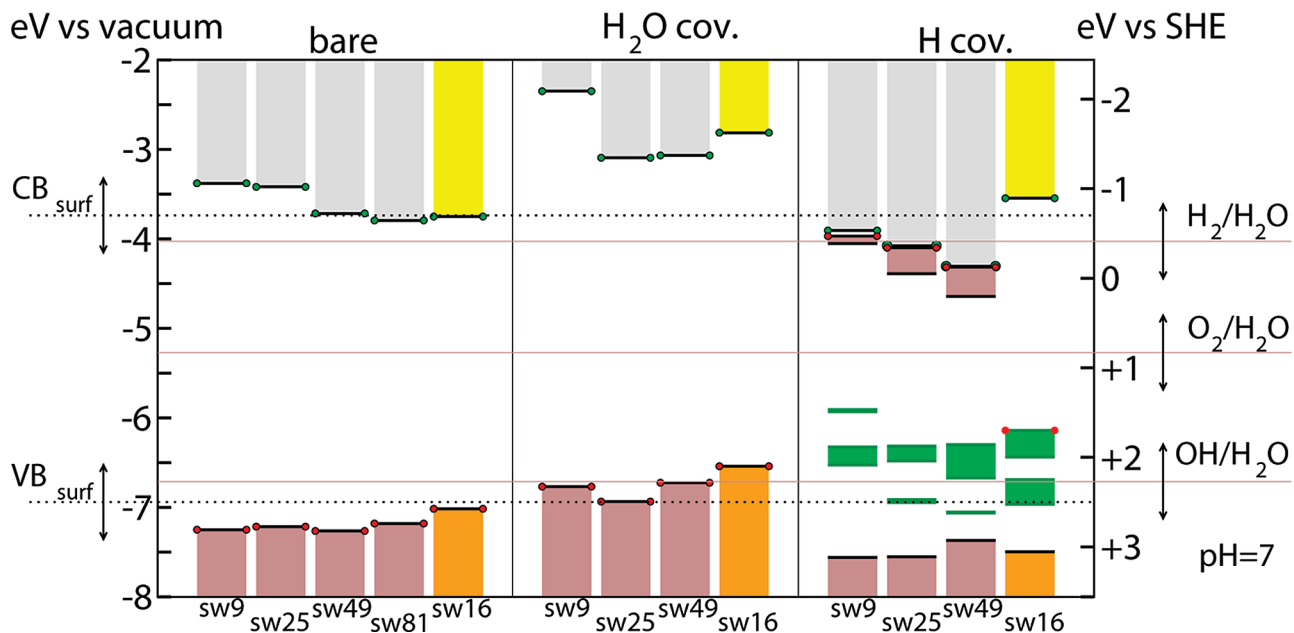
energy and hence to an electrochemical scale by means of cylindrical averages of the electrostatic potential, as defined in the section of the computational details. Moreover a rigid shift of the conduction bands has been applied to correct the DFT underestimation of the band gap of the semiconductive NWs, as detailed later. Thus we analyzed for the case of TiO<sub>2</sub> NWs the effect of size reduction, the determination of the h<sup>+</sup> acceptor site, and the capability of hydrogen sensing.

Figure 5 reports the VBM, the CBMs, and in-gap states energies of the NWs. To give a direct comparison of these energies with experimental data we scaled the graph with respect to the vacuum reference (on the left) and to the standard hydrogen electrode (on the right), and we also reported the highest occupied molecular orbital (HOMO) energy obtained with an ultraviolet photoelectron spectroscopy (UPS) measurement on a nanocrystalline TiO<sub>2</sub> thin film<sup>77</sup> (labeled as VB<sub>surf</sub>). Horizontal lines refer to the redox potentials at pH 7 of the species involved in the water splitting process.<sup>78</sup> The respective vertical arrows set the energy range in which these energies change by changing the pH of the solution (toward more positive values with decreasing pH and vice versa for increasing pH).

We found the VBM of all the bare NWs to fall in the range -7.26 to -7.01 eV (see Table 2). By considering that our bare systems are isolated NWs, we can compare this energy range with the UPS measure of -6.94 eV obtained in vacuum by Snook et al. on nanocrystalline TiO<sub>2</sub> thin films.<sup>77</sup> UV-vis absorption spectrum gives a VBM value of -7.4 eV for TiO<sub>2</sub> nanorods surface capped with conjugate polymers,<sup>79</sup> which however shift the VBM due to charge transfer at the interface. Comparison is also possible with cyclic voltammetric measurements that gave a VBM value of -6.9 eV for surface-capped TiO<sub>2</sub> nanocrystals,<sup>80</sup> whereas the anatase single crystal value lies around -7.13 eV at pH 7.<sup>81</sup> In this case, the VBM is extrapolated by measuring the flat band potential, which matches the apparent Fermi energy of the sample.

All these values unveil that the NWs do not undergo a sensible variation of the VBM energy, also for the case of the thinnest sw9 NW. Thus an increase of the oxidant capability of TiO<sub>2</sub> h<sup>+</sup> cannot be achieved merely by size reduction of NWs. In fact, the VBM energy difference between the thinnest sw9 and the largest sw81 NW is 0.07 eV. Room for tuning the VBM energy can instead be connected to the morphology of the NWs, since first type NWs, elongated in the [001] direction, have a VBM energy at least 0.17 eV lower than the second type NW, grown along the [010] direction. Anyway all the VBM energies are more positive (at least +2.57 eV) than the redox potential of the O<sub>2</sub>/H<sub>2</sub>O couple (+0.83 eV, pH = 7), which means that all NWs are able to support oxidation of H<sub>2</sub>O by h<sup>+</sup> donation.

To produce the reaction of the water splitting it is also necessary that the H<sub>2</sub> reduction potential is less negative than the CBM energy of the NWs. Bulk rutile has a VBM energy essentially coincident with the reversible hydrogen potential, whereas for bulk anatase is more negative by 0.20 eV.<sup>83</sup> Therefore anatase is the only TiO<sub>2</sub> crystal phase thermodynamically able to induce the water photoelectrolysis.<sup>81</sup> As discussed in the previous section, DFT typically underestimates the band gap of semiconductors so that a direct comparison of the CBM energies in Figure 5 with experiments is not possible without applying a rigid shift (1.12 eV) to the empty bands energies. This procedure would match the calculated bulk band gap (2.08 eV) and the experimental one (3.2 eV) and it has been already applied to the TiO<sub>2</sub> semiconductor.<sup>74,84,85</sup> The shift unveils that all NWs CBM energies lie above -0.65 eV vs SHE, which is 0.24 eV more negative than the H<sup>+</sup>/H<sub>2</sub> reduction potential



**Figure 5.** Band line-up of the NWs in the gap region. Brown bars refer to occupied states (orange for the second type NW elongated in the [010] direction) and gray bars refer to empty states (yellow bars for the second type NW). Green bars refer to hydrogen-induced in-gap states. Red circles refer to the HOMO energy level whereas green circles refer to the LUMO energy level. The dotted horizontal lines are the experimental HOMO ( $\text{VB}_{\text{surf}}$ ) and LUMO ( $\text{CB}_{\text{surf}}$ ) energy levels from ref 77. Continuous horizontal lines refer to the energy value of relevant redox potential couples at pH = 7 taken from ref 78. Their respective vertical lines span the energy range of variation with the pH. On the right the energy scale is relative to the standard hydrogen electrode (SHE). All the CBM energies of semiconductive NWs are shifted of +1.12 eV to account for the DFT underestimation of the band gap of semiconductive materials.

(−0.413 eV<sup>78</sup>). All the bare NWs are thus found to be able to produce a complete water-splitting reaction by oxidation of water at the surface and reduction of protons at the cell cathode.

The morphology of the NWs, also in this case, can play a role in determining the ability of the nanostructure to efficiently produce the reaction, since the second type NW (sw16) has a CBM energy close to the larger first type NWs (sw49 and sw81) and to the experimental CBM of nanocrystalline thin films,<sup>77</sup> but as stated before the sw16 VBM energy is about 0.2 eV higher than those of all the first type NWs. Therefore we expect an overall lower yield of the second type NW with respect to the first type, for NWs of the same size.

The last result deals with the effect of the size on the first type NWs, elongated in the [001] direction. The respective CBM energy is shifted to higher negative redox potential values as the size reduces, such that the thinnest sw9 has a CBM energy 0.41 eV more negative than that of sw81. This directly leads to infer that as the diameter of the [001] NWs decreases the ability to reduce protons to produce molecular hydrogen increases. Hence the anatase [001] NWs show an increasing efficiency in the water splitting as a consequence of the size confinement.

**Pathways of Reactions at the Surface of the NWs.** In this section, we discuss an unsolved problem in the photocatalytic activity of  $\text{TiO}_2$ , that is, the nature of the  $\text{h}^+$  trap responsible for the oxidation of reactants.<sup>83</sup> There is consensus on the fact that recombination of photocharges is delayed by trapping in localized states, from which photocharges are transferred to dissolved reactants.<sup>83,86</sup> However the hole trap site is not yet unambiguously determined, since it has been assigned to terminal hydroxyl radicals,<sup>86,87</sup> lattice oxygens,<sup>88</sup> subsurface oxygens,<sup>89</sup> and surface oxygen radicals.<sup>82,90</sup> Here we consider our water coverage of the NWs as a model configuration for the hydroxyl termination, where the hydrogen-covered oxygen of the bare NW ( $\text{Ti}-\text{OH}-\text{Ti}$ ) represents an acidic site while the hydroxyl group that covers undercoordinated Ti represents

a basic site ( $\text{Ti}-\text{O}-\text{Ti}-\text{OH}$ ).<sup>82</sup> This surface configuration is based on the assumption that  $\text{TiO}_2$  nanostructures are more hydroxylated than macroscopic surfaces, given the stabilizing role of the hydroxyl group.<sup>58,59</sup> Therefore it simulates a generic configuration of a stable surface covered NW.

As shown in Figure 5, the VBM and CBM energies of the  $\text{H}_2\text{O}$  covered NWs are upward shifted in comparison to the bare case. It is a consequence of the Nernstian dependence of the band edge energies from the pH, which is valid for most oxide semiconductor/aqueous solution interfaces<sup>91</sup> and is found to persist over a wide range of pH for nanocrystalline  $\text{TiO}_2$ .<sup>92</sup> It is essentially ascribed to a surface acid–base equilibrium where charge is transferred creating an accumulation layer in the solid; the bands undergo an upward bending if excess electrons are accommodated on the surface whereas downward bending is a consequence of positive excess charge.<sup>83,91</sup> Our model NWs are subject to the same shift, which is predominantly due to the basic behavior of the terminal hydroxyl groups ( $\text{Ti}-\text{OH}$ ), where excess electronic charge is transferred from bound Ti atoms. This leads to consider our surface configuration as a reliable model for NWs in basic solution and shows that the general model employed for the  $\text{TiO}_2$  semiconductor holds through the nanometer scale. Thus a first result is the effective ability of the hydroxyl groups adsorbed on the surface of NWs to attract excess electronic charge. Hence it is possible that conduction band electrons are scavenged by the presence of such terminal groups as experimentally reported for  $\text{TiO}_2$  nanocrystals.<sup>76</sup>

The VBM energies of the hydrated NWs lie around the water oxidation potential to hydroxyls (2.27 eV vs SHE, pH = 7)<sup>78</sup> as reported in Table 2. This means that the overall effect of terminal  $\text{Ti}-\text{OH}$  groups is to lower the oxidizing potential of the NWs, if they constitute stable radicals in acidic environments. On the other hand, the upward bending of the CBM energies increases the reducing potential of photoelectrons, which are able to form superoxide  $\text{O}_2^-$  and hydrogen peroxide

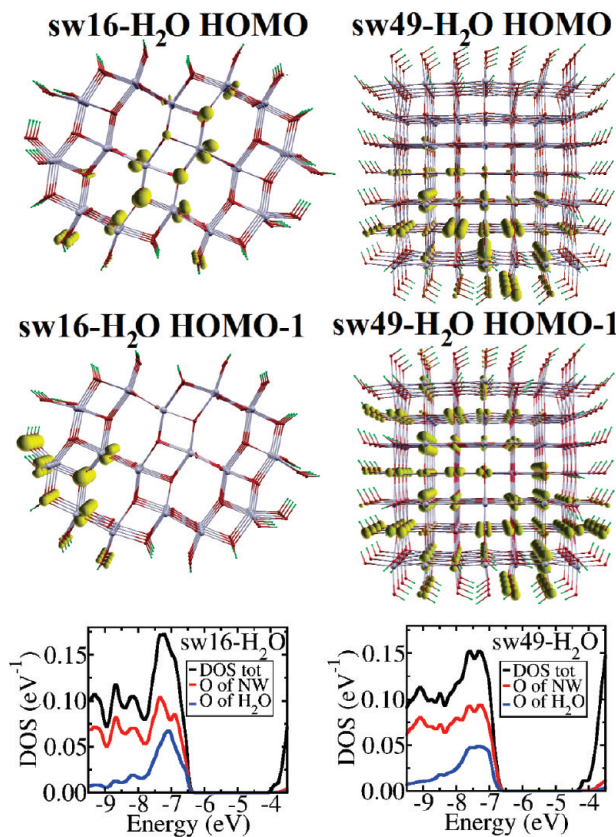


**Figure 6.** Charge density contour plots (10% of the maximum value) of the HOMO and HOMO-1 states of the hydrated sw16 NW on the left and the hydrated sw49 NW on the right. In the bottom panels the respective total DOS (black line) is projected on the oxygen orbitals belonging to the NW (red line) and to the water molecules (blue line). The complete set of graphs is provided in the Supporting Information, Figure 4.

H<sub>2</sub>O<sub>2</sub>. Two questions that are debated in literature on the activity of TiO<sub>2</sub> surfaces and nanocrystalline assemblies can now be discussed in the case of TiO<sub>2</sub> NWs.<sup>90</sup> (i) Can the photogenerated TiO<sub>2</sub> VB hole oxidize the terminal OH radical? (ii) Which condition allows the production of free OH species participating in the primary oxidation of organic compounds? The first question can be addressed by studying the nature of the top VB states. The analysis of the DOS and of the charge distribution of states reveals that the highest-occupied states are indeed O 2p as expected for TiO<sub>2</sub>, but their spatial distribution involves both oxygens from the hydroxyl groups and oxygens of the NWs (see Figure 6). This is because the energy range of the OH 2p states overlaps with that of the O 2p states of the NWs. Hence a clear distinction of the final hole trap between hydroxyl termination and subsurface oxygen is not possible for the thinnest imaginable anatase NWs. This result points out that the subsurface oxygens can be expected to play the major role in trapping the holes, based on the following remarks. (i) The degree of hydroxylation of TiO<sub>2</sub> surfaces is inversely proportional to the size of the material. Our hydrated NWs (as being of the smallest size) are completely hydroxylated and thus model an extreme configuration, where all the available surface sites are hydroxylated. (ii) Although such a complete hydroxylation, the DOS maximum peak of the OH 2p states is at least 0.30 eV under the VBM for all the NWs, which means that these states cannot be considered as deep hole traps. (iii) Upon increasing the size of the NWs to a macroscopic scale, the ratio between surface hydroxyls and subsurface oxygens will turn more and more in favor of the latter, such that the major fraction

of available hole traps will be constituted of subsurface oxygens. These observations can explain the reason why holes are found to be trapped at surface or subsurface oxygens in TiO<sub>2</sub> colloids and films,<sup>89,90</sup> whereas they are found to be trapped at surface oxygen radicals or terminal hydroxyls in TiO<sub>2</sub> nanoparticles.<sup>82,86,87</sup> The second question dealing with the availability of free OH species can be addressed following the picture given by Salvador.<sup>90</sup> If the surface of TiO<sub>2</sub> NWs is highly hydroxylated in a wide range of pH, the ability to oxidize water can decrease but the upward shift of the CBM energies increases the reduction of dissolved oxygen to superoxide and hydrogen peroxide that ultimately react to produce free OH species. We consider this dynamics to be more feasible for hydroxylated NWs exposed to gaseous environment due to the limitations that our model systems have to simulate a liquid environment.

**Hydrogen Sensing Ability of the NWs.** This last section deals with the possibility to employ TiO<sub>2</sub> NWs as hydrogen sensors. Experiments reveal that TiO<sub>2</sub> nanotubes<sup>54,93</sup> and mesowires<sup>55</sup> show an increase of the conductance upon exposure to hydrogen gas, which can be of some orders of magnitude<sup>94</sup> and can lead to the highest variation of the electrical properties of a material, to any gas, ever shown.<sup>95</sup> The main mechanism is ascribed to the chemisorption of the dissociated hydrogen molecules at the surface due to the high electrical variation, velocity, and reversibility of the sensing process.<sup>96</sup> Measurements in acid medium show that the resistivity is so low that cannot be reliably measured and a negative bias potential is not needed.<sup>93</sup> Our hydrogenated model systems can fit an analogous surface configuration as the one proposed with dissociated hydrogen molecules covering the surface atoms of the NWs.

As shown in Figure 5, all the H-covered NWs present in-gap states (green bars) above the VBM energy of the TiO<sub>2</sub> O 2p states. The space charge distribution of these states is surface localized on the titanium-bonded hydrogen atoms. The VBM energies are downward shifted with respect to the bare case (in the range -7.56 to -7.37 eV vs vacuum), as expected in acidic conditions where an excess partial positive charge accommodates at the surface (see Table 2). The most interesting result concerns the bottom of the conduction bands. The first type NWs elongated in the [001] direction have occupied states close in energy to the empty states, showing a gap in the range 10–60 meV. The spatial charge distribution of these states is not localized to single atoms but is conductive-like with an exclusive Ti 3d atomic character that is typical of the TiO<sub>2</sub> conduction bands (see Figure 7). Thus it is possible to conclude that TiO<sub>2</sub> NWs can show an increase of the conductance due to the injection of electrons in the conduction bands following hydrogen chemisorption at the surface. From the nature of these occupied states below the CBM, that is, the Ti 3d atomic character, the delocalization of the charge density, and the dispersion of the bands, it is possible to infer that these occupied bands are indistinguishable from the conduction bands of the TiO<sub>2</sub> bare NWs. At the end, the adsorption of hydrogen leads to the formation of a space charge layer that induces the band bending of the energy levels of the NW. The depth of this bending is typically of the order of few nanometers but longer than the diameter of our NWs. Hence the potential shift induced by the space charge layer extends throughout the NW in such a way to equilibrate the NW Fermi energy with the H<sup>+</sup> surface state energy. From an electrochemical viewpoint, the H<sup>+</sup> (aq)/H<sub>2</sub> (g) energy is in the range -0.413–0 eV vs SHE according to the degree of acidity of the pH, and in fact the occupied states energies lie in the range -0.47–0.20 eV vs SHE.

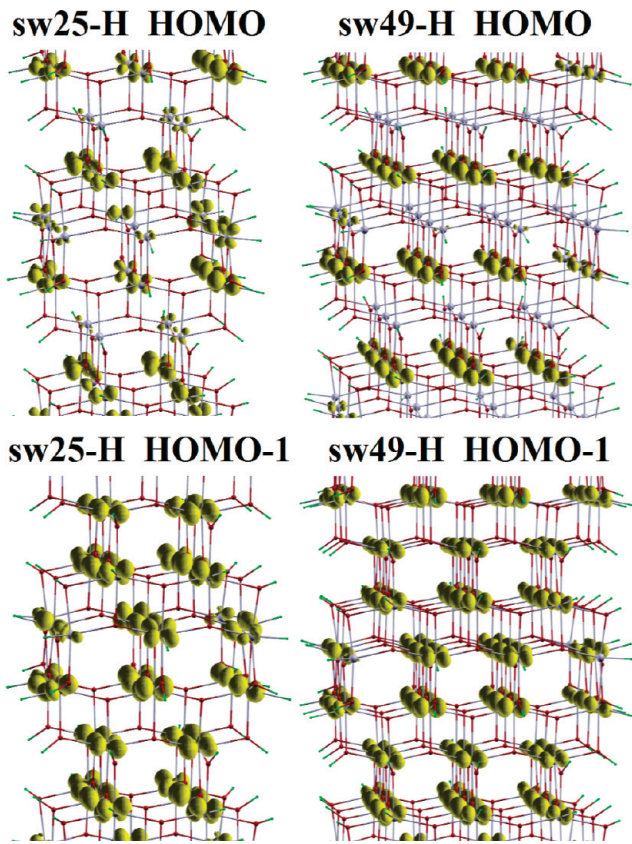


**Figure 7.** Charge density contour plots (10% of the maximum value) of the HOMO and HOMO-1 states of the hydrogenated sw25 NW on the left and the hydrogenated sw49 NW on the right. The charge densities are not spatially localized but spread throughout the NWs.

The second interesting result is related to the dependence of the presence of occupied states in the CBM energy region from the surface morphology. The second type NW elongated in the [010] direction does not show such states, but only the decrease of the band gap due to the in-gap states above the VBM. Hence we do not expect the same degree of sensitivity to hydrogen gas for this type of NW, although it has barely the same size of the larger first type NWs. This result highlights the importance of the structural features of low dimensional materials in determining their overall properties and applicability. At the nanoscale the presence of specific sites plays a fundamental role since the relative amount of each type of active site can be increased by tuning the morphology of the nanostructure.

**Relative Stability Analysis.** The knowledge of the expected stable configurations can be of particular relevance for the choice of the NWs to design and to synthesize. In this last section, we discuss the relative energetic stability of the studied NWs. We calculated the formation energy of a NW as defined by the equation  $E_f = E_{\text{tot}} - M_x \mu_x - N \mu_{\text{TiO}_2}$ , where  $E_{\text{tot}}$  is the total energy of the NW,  $M_x$  is the number of covering molecules having chemical potential  $\mu_x$  ( $\mu_{\text{H}_2} = -31.80$  eV,  $= -469.51$  eV),  $N$  is the number of  $\text{TiO}_2$  units (with chemical potential  $\mu_{\text{TiO}_2}$ ). The chemical potentials are chosen as the total energy of the correspondent isolated molecules. The energy required to cover the surface with a given adsorbate is given by the equation  $E_c = E_{\text{tot}} - M_x \mu_x - E_{\text{tot}}^{\text{bare}}$ , where  $E_{\text{tot}}$  is the total energy of the covered NW,  $E_{\text{tot}}^{\text{bare}}$  is the total energy of the correspondent bare NW, and  $M$  is the total number of covering molecules.

As depicted in Figure 8a the formation energy per  $\text{TiO}_2$  unit ( $E_f/N_{\text{TiO}_2}$ ) of all the NWs is negative, which means that their molecular constituents gain stability upon NW formation.

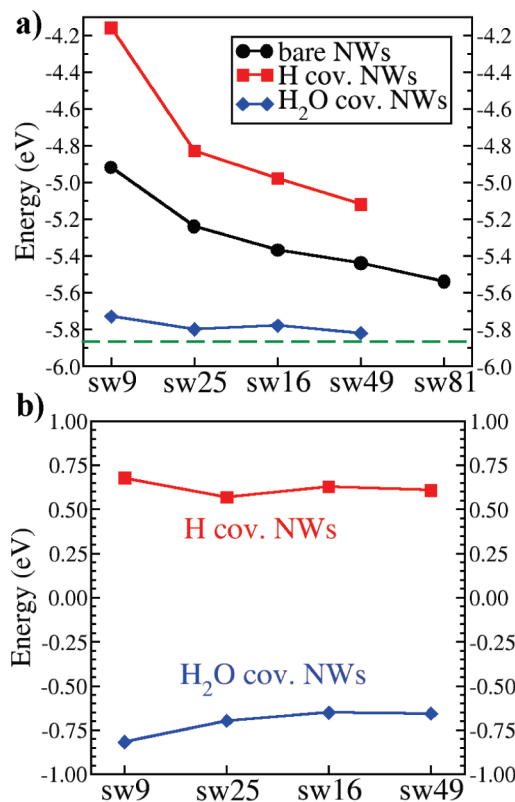


**Figure 8.** (a) Plot of the formation energy per molecule of the NWs as function of the diameter size. The black curve refers to bare NWs, the red curve refers to hydrogenated NWs, and the blue one refers to hydrated NWs. The green dotted line is the formation energy per  $\text{TiO}_2$  unit of the bulk anatase. (b) Plot of the adsorption energy per adsorbate molecule as function of the diameter size. The red curve refers to the  $\text{H}_2$  adsorption energy and the blue curve refers to the water adsorption energy.

Furthermore, the stability of the NWs increases on increasing the size. This trend is more appreciable for the bare and hydrogenated NWs whose formation energy is thus found to be favored by the size growth. The hydrated NWs are the most stable systems with formation energies that are close to the bulk value (the maximum energy difference is less than 0.14 eV). Hence the surface configuration reveals its importance in determining the feasibility of a NW also in terms of energetic stability. In fact, given a bare NW, the hydration coverage leads always to the most stable system whereas hydrogenation leads to the least stable system. Figure 8b, reporting the coverage energy defined above per adsorbing molecule ( $E_{\text{cov}}/M$ ), shows that the dissociative adsorption of hydrogen molecules is unfavored for all the NWs. This configuration is thus highly reactive and can fit for applications in hydrogen rich gaseous environments. On the other hand, the dissociation of the water molecule at the surface of  $\text{TiO}_2$  NWs is a stabilizing process (negative coverage energies in Figure 8b) since it is able to fill oxygen vacancies, to close the octahedral coordination of terminal titanium atoms, and to preserve a high crystallinity through the smallest  $\text{TiO}_2$  NWs that can be synthesized. The stabilization of the bare NWs upon dissociative adsorption of water is more pronounced for the thinnest NWs.

Our result confirms the possibility to find a consistent amount of terminal hydroxyl groups on the surface of  $\text{TiO}_2$  NWs as experimentally reported.<sup>35,57</sup> We can predict that the stabilizing role of the water coverage experimentally found for  $\text{TiO}_2$  NCs<sup>59</sup> also stands in the case of 1D NWs. At the end we found that the dissociative adsorption of water forms strong bonds at the

surface thus extending the experimental results obtained for TiO<sub>2</sub> NCs<sup>58,59</sup> to the one-dimensional case.

## Conclusions

In this work we presented a detailed investigation of the structural and electronic properties of 1D anatase NWs through first-principles calculations. We showed that these properties depend on the diameter size, on the surface coverage, and on the morphology (namely, growing direction and lateral surfaces) of the NWs. These informations can be useful to outline a theoretical background of knowledge, readily available for the experimental research on new TiO<sub>2</sub> nanomaterials and devices. We also proposed an interpretation of some currently debated experimental findings on TiO<sub>2</sub> nanostructures. The main results of this study are summarized in the following: (1) The bare NWs have an inward contraction that decreases their size whereas the surface coverage induces an outward expansion. Hence the final configuration is the result of two competing phenomena. On one hand, the own trend of TiO<sub>2</sub> anatase to exhibit volume reduction on decreasing the diameter size. On the other hand, the presence of specific adsorbates can compensate or even reverse this trend leading to expansion, which is typical of nanoparticles shorter than 10 nm.<sup>72</sup> In fact, the surface atoms are found to undergo the largest displacements depending on the kind of covering species. Thus as the size increases the effects of the surface deformations lose their weight in determining the overall configuration. (2) The size increase and, more importantly, the surface coverage induce a better (more “ordered”) structural organization of the NWs. Thus it is possible to select specific adsorbates that help in obtaining well-ordered and crystallized NWs. (3) NWs grown along the [010] direction and with (101) and (001) derived surfaces have a higher crystallinity than NWs grown along the [001] direction and with (100) and (010) surfaces. Hence, by changing the exposed surfaces and the growth direction it is possible to tune the NW crystalline strength against variations of the size and of the surface configuration. (4) Bare and hydrated NWs show the band gap blue shift due to the size confinement. The band gap shift depends on the morphology since the bare NWs grown along the [010] direction do not show an appreciable variation of the gap as the NWs of comparable size elongated in the [001] direction. The band gap blue shift is a function of the crystallinity of the NW, since all the hydrated NWs have a higher shift than the respective bare counterparts. (5) The charge densities of the electronic states lying in the “bulk” band gap region are found to involve the surface atoms. Thus, we expect that TiO<sub>2</sub> NWs show a high photocatalytic activity. The surface hydration of the NWs can tune the availability of internal channels for the transport of photoelectrons. This result can be generalized by stating that it is possible to find functionalizing adsorbates that increase the charge transport properties of the NWs conduction bands. (6) The bare NWs have VBM and CBM energies that allow, in principle, the production of H<sub>2</sub> and O<sub>2</sub> from the water splitting. This ability is found to increase on decreasing the size of the NWs elongated in the [001] direction. Thus the quantum confinement can effectively be used to enhance the photocatalytic performances of 1D TiO<sub>2</sub> nanostructures. (7) The surface hydroxyl groups cannot be considered as deep hole traps in the oxidation reactions of TiO<sub>2</sub> NWs. The O 2p electronic states of these groups have binding energies that overlap with those of the O 2p states coming from the surface region of the TiO<sub>2</sub> NWs. (8) Surface hydrogenation leads to occupied states at the bottom of the CBM energies of the NWs grown in the [001] direction. Thus we expect that TiO<sub>2</sub> NWs

increase their conductance upon surface hydrogen chemisorption and be designed as hydrogen sensors as already proved for TiO<sub>2</sub> nanotubes.<sup>54</sup> However, the TiO<sub>2</sub> NWs sensing ability can be a function of the morphology, since the NW grown in the [010] direction does not show such occupied states. (9) At the end, we found that the surface hydration is the most stable configuration for all the considered NWs. This result highlights the importance of the stabilizing role played by the terminal hydroxyl groups in the synthesis process or in the working environment of the TiO<sub>2</sub> NWs.

**Acknowledgment.** A.I. acknowledges CNISM for the financial support. Financial support from project MIUR-PRIN-2007 and computational resources from CINECA (“Progetti Super-calcolo 2008”) are gratefully acknowledged.

**Supporting Information Available:** We provide the reader with further figures to complete the results shown in this article. This material is available free of charge via the Internet at <http://pubs.acs.org>.

## References and Notes

- (1) Diebold, U. *Surf. Sci. Rep.* **2003**, *48*, 53.
- (2) Carp, O.; Huisman, C. L.; Reller, A. *Prog. Solid State Chem.* **2004**, *32*, 33.
- (3) Fernández-García, M.; Martínez-Arias, A.; Hanson, J. C.; Rodriguez, J. A. *Chem. Rev.* **2004**, *104*, 4063.
- (4) Chen, X.; Mao, S. S. *Chem. Rev.* **2007**, *107*, 2891.
- (5) Adachi, M.; Murata, Y.; Takao, J.; Jiu, J.; Sakamoto, M.; Wang, F. *J. Am. Chem. Soc.* **2004**, *126*, 14943.
- (6) Mao, Y.; Kanungo, M.; Hemraj-Benny, T.; Wong, S. S. *J. Phys. Chem. B* **2006**, *110*, 702.
- (7) Yu, H.; Yu, J.; Cheng, B. *J. Mol. Catal. A: Chem.* **2006**, *253*, 99.
- (8) Wang, Q.; Wen, Z.; Li, J. *Inorg. Chem.* **2006**, *45*, 6944.
- (9) Koo, B.; Park, J.; Kim, Y.; Choi, S.-H.; Sung, Y.-E.; Heon, T. J. *Phys. Chem. B* **2006**, *110*, 24318.
- (10) Kitano, M.; Mitsui, R.; Eddy, D. R.; El-Bahy, Z. M. A.; Matsuoka, M.; Ueshima, M.; Anpo, M. *Catal. Lett.* **2007**, *119*, 217.
- (11) Feng, X.; Shankar, K.; Varghese, O. K.; Paulose, M.; Latempa, T. J.; Grimes, C. A. *Nano Lett.* **2008**, *8*, 3781.
- (12) Limmer, S.; Cao, G. *Adv. Mater.* **2003**, *15*, 427.
- (13) Yu, K.; Zhao, J.; Zhao, X.; Ding, X.; Zhu, Y.; Wang, Z. *Mater. Lett.* **2005**, *59*, 2676.
- (14) Pol, V. G.; Langzam, Y.; Zaban, A. *Langmuir* **2007**, *23*, 11211.
- (15) Attar, A. S.; Ghamsari, M. S.; Hajiesmaeilbaigi, F.; Mirdamadi, S.; Katagiri, K.; Koumoto, K. *J. Phys. D: Appl. Phys.* **2008**, *41*, 155318.
- (16) Shim, H.-S.; Na, S.-I.; Nam, S. H.; Ahn, H.-J.; Kim, H. J.; Kim, D.-Y.; Kim, W. B. *Appl. Phys. Lett.* **2008**, *92*, 183107.
- (17) Dürr, M.; Schmid, A.; Obermaier, M.; Rosselli, S.; Yasuda, A.; Nelles, G. *Nat. Mater.* **2005**, *4*, 607.
- (18) Tan, B.; Wu, Y. *J. Phys. Chem. B* **2006**, *110*, 15932.
- (19) Kang, S. H.; Choi, S.-H.; Kang, M.-S.; Kim, J.-Y.; Kim, H.-S.; Heon, T.; Sung, Y.-E. *Adv. Mater.* **2008**, *20*, 54.
- (20) Centi, G.; Perathoner, S. *Catal.* **2007**, *20*, 367.
- (21) Zhu, K.; Vinzant, T. B.; Neale, N. R.; Frank, A. J. *Nano Lett.* **2007**, *7*, 3739.
- (22) Wang, R.; Ruan, C.; Kanayeva, D.; Lassiter, K.; Li, Y. *Nano Lett.* **2008**, *8*, 2625.
- (23) Enyashin, A. N.; Seifert, G. *Phys. Status Solidi B* **2005**, *242*, 1361.
- (24) Allen, P. B. *Nano Lett.* **2007**, *7*, 6.
- (25) Alvarez-Ramirez, F.; Ruiz-Morales, Y. *Chem. Mater.* **2007**, *19*, 2947.
- (26) Zhang, D.; Liu, P.; Liu, C. *J. Phys. Chem. C* **2008**, *112*, 16729.
- (27) Meng, S.; Ren, J.; Kaxiras, E. *Nano Lett.* **2008**, *8*, 3266.
- (28) Polleux, J.; Pinna, N.; Antonietti, M.; Hesse, C.; Wild, U.; Schlögl, R.; Niederberger, M. *Chem.—Eur. J.* **2005**, *11*, 3541.
- (29) Niederberger, M.; Garnweinert, G. *Chem.—Eur. J.* **2006**, *12*, 7282.
- (30) Jiu, J.; Isoda, S.; Wang, F.; Adachi, M. *J. Phys. Chem. B* **2006**, *110*, 2087.
- (31) Iacomo, A.; Canale, G.; Ninno, D.; Marri, I.; Ossicini, S. *Phys. Rev. B* **2008**, *78*, 075405.
- (32) Liu, C.; Yang, S. *ACS Nano* **2009**, *3*, 1025.
- (33) Polleux, J.; Pinna, N.; Antonietti, M.; Niederberger, M. *Adv. Mater.* **2004**, *16*, 436.
- (34) Gao, X.; Zhu, H.; Pan, G.; Ye, S.; Lan, Y.; Wu, F.; Song, D. *J. Phys. Chem. B* **2004**, *108*, 2868.

- (35) Joo, J.; Kwon, S. G.; Yu, T.; Cho, M.; Lee, J.; Yoon, J.; Hyeon, T. *J. Phys. Chem. B* **2005**, *109*, 15297.
- (36) Wei, Q.; Hirota, K.; Tajima, K.; Hashimoto, K. *Chem. Mater.* **2006**, *18*, 5080.
- (37) Daoud, W.; Pang, G. K. H. *J. Phys. Chem. B* **2006**, *110*, 25746.
- (38) Berger, T.; Lana-Villarreal, T.; Monllor-Satoca, D.; Gómez, R. *J. Phys. Chem. C* **2008**, *112*, 15920.
- (39) Chen, L. X.; Rajh, T.; Wang, Z.; Thurnauer, M. C. *J. Phys. Chem. B* **1997**, *101*, 10688.
- (40) Luca, V.; Djajanti, S.; Howe, R. F. *J. Phys. Chem. B* **1998**, *102*, 10650.
- (41) Yeung, K. L.; Maira, A. J.; Stoltz, J.; Hung, E.; Ho, N. K.; Wei, A. C.; Soria, J.; Chao, K.; Yue, P. L. *J. Phys. Chem. B* **2002**, *106*, 4608.
- (42) Yeung, K. L.; Yau, S. T.; Maira, A. J.; Coronado, J. M.; Soria, J.; Yue, P. L. *J. Catal.* **2003**, *219*, 107.
- (43) Serpone, N.; Lawless, D.; Khairutdinov, R. *J. Phys. Chem.* **1995**, *99*, 16646.
- (44) Monticone, S.; Tufeu, R.; Kanaev, A. V.; Scolan, E.; Sanchez, C. *Appl. Surf. Sci.* **2000**, *162–163*, 565.
- (45) Kormann, C.; Bahnenmann, D. W.; Hoffmann, M. R. *J. Phys. Chem.* **1988**, *92*, 5196.
- (46) Anpo, M.; Shima, T.; Kodama, S.; Kubokawa, Y. *J. Phys. Chem.* **1987**, *91*, 4305.
- (47) Yuwono, A. H.; Xue, J.; Wang, J.; Elim, H. I.; Ji, W.; Li, Y.; White, T. J. *J. Mater. Chem.* **2003**, *13*, 1475.
- (48) Pan, D.; Zhao, N.; Wang, Q.; Jiang, S.; Ji, X.; An, L. *Adv. Mater.* **2005**, *17*, 1991.
- (49) Satoh, N.; Nakashima, T.; Kamiruka, K.; Yamamoto, K. *Nature (London)* **2008**, *3*, 106.
- (50) Lei, Y.; Zhang, L. D.; Fan, J. C. *Chem. Phys. Lett.* **2001**, *338*, 231.
- (51) Das, K.; Panda, S. K.; Chaudhuri, S. *J. Cryst. Grow.* **2008**, *310*, 3792.
- (52) Khan, S. U. M.; Sultana, T. *Sol. Energy Mater. Sol. Cells* **2003**, *76*, 211.
- (53) Ni, M.; Leung, M. K. H.; Leung, D. Y. C.; Sumathy, K. *Renewable Sustainable Energy Rev.* **2007**, *11*, 401.
- (54) Varghese, O. K.; Gong, D.; Paulose, M.; Ong, K. G.; Dickey, E. C.; Grimes, C. A. *Adv. Mater.* **2003**, *15*, 624.
- (55) Sysoev, V. V.; Button, B. K.; Wepsiec, K.; Dmitriev, S.; Kolmakov, A. *Nano Lett.* **2006**, *6*, 1584.
- (56) Jitputti, J.; Suzuki, Y.; Yoshikawa, S. *Catal. Comm.* **2008**, *9*, 1265.
- (57) Dong, F.; Zhao, W.; Wu, Z. *Nanotechnology* **2008**, *19*, 365607.
- (58) Soria, J.; Sanz, J.; Sobrados, I.; Coronado, J. M.; Maira, A. J.; Hernández-Alonso, M. D.; Fresno, F. *J. Phys. Chem. C* **2007**, *111*, 10590.
- (59) Levchenko, A. A.; Li, G.; Boerio-Goates, J.; Woodfield, B. F.; Navrotksy, A. *Chem. Mater.* **2006**, *18*, 6324.
- (60) Giannozzi, P.; Baroni, S.; Bonini, N.; Calandra, M.; Car, R.; Cavazzoni, C.; Ceresoli, D.; Chiarotti, G. L.; Cococcioni, M.; Dabo, I.; Dal Corso, A.; Fabris, S.; Fratesi, G.; de Gironcoli, S.; Gebauer, R.; Gerstmann, U.; Gougaoussis, C.; Kokalj, A.; Lazzeri, M.; Martin-Samos, L.; Marzari, N.; Mauri, F.; Mazzarello, R.; Paolini, S.; Pasquarello, A.; Paulatto, L.; Sbraccia, C.; Scandolo, S.; Sclauzero, G.; Seitsonen, A. P.; Smogunov, A.; Umari, P.; Wentzcovitch, R. M. *J. Phys.: Condens. Matter* **2009**, *21*, 395502.
- (61) Perdew, J. P.; Wang, Y. *Phys. Rev. B* **1992**, *45*, 13244.
- (62) Vanderbilt, D. *Phys. Rev. B* **1990**, *41*, 7892.
- (63) Monkhorst, H. J.; Pack, J. D. *Phys. Rev. B* **1976**, *13*, 5188.
- (64) Mordecai, A. *Nonlinear Programming: Analysis and Methods*; Dover Publishing: Mineola, NY, 2003.
- (65) Burdett, J. K.; Hughbanks, T.; Miller, G. J.; Richardson, J. W., Jr.; Smith, J. V. *J. Am. Chem. Soc.* **1987**, *109*, 12.
- (66) Shklover, V.; Nazeeruddin, M.-K.; Zakeeruddin, S. M.; Barbé, C.; Kay, A.; Haibach, T.; Steurer, W.; Hermann, R.; Nissen, H.-U.; Grätzel, M. *Chem. Mater.* **1997**, *9*, 430.
- (67) Nian, J.-N.; Teng, H. *J. Phys. Chem. B* **2006**, *110*, 4193.
- (68) Wen, P.; Itoh, H.; Tang, W.; Feng, Q. *Langmuir* **2007**, *23*, 11782.
- (69) Caputo, G.; Nobile, C.; Kipp, T.; Blasi, L.; Grillo, V.; Carlino, E.; Manna, L.; Cingolani, R.; Cozzoli, P. D.; Athanassiou, A. *J. Phys. Chem. C* **2008**, *112*, 701.
- (70) Barnard, A. S.; Zapol, P. *Phys. Rev. B* **2004**, *70*, 235403.
- (71) Swamy, V.; Menzies, D.; Muddle, B. C.; Kuznetsov, A.; Dubrovinsky, L. S.; Dai, Q.; Dmitriev, V. *Appl. Phys. Lett.* **2006**, *88*, 243103.
- (72) Luca, V. *J. Phys. Chem. C* **2009**, *113*, 6367.
- (73) Mo, S.-D.; Ching, W. Y. *Phys. Rev. B* **1995**, *51*, 13023.
- (74) Asahi, R.; Taga, Y.; Mannstadt, W.; Freeman, A. *J. Phys. Rev. B* **2000**, *61*, 7459.
- (75) Thulin, L.; Guerra, J. *Phys. Rev. B* **2008**, *77*, 195112.
- (76) Panayotov, D. A.; Yates, J. T., Jr. *Chem. Phys. Lett.* **2005**, *410*, 11.
- (77) Snook, J. H.; Samuelson, L. A.; Kumar, J.; Kim, Y.-G.; Whitten, J. E. *Org. Electron.* **2005**, *6*, 55.
- (78) Fujishima, A.; Rao, T. N.; Tryk, D. A. *J. Photochem. Photobiol. C* **2003**, *1*, 1.
- (79) Lin, Y.-T.; Zeng, T.-W.; Lai, W.-Z.; Chen, C.-W.; Lin, Y.-Y.; Chang, Y.-S.; Su, W.-F. *Nanotechnology* **2006**, *17*, 5781.
- (80) Petrella, A.; Tamborra, M.; Curri, M. L.; Cosma, P.; Striccoli, M.; Cozzoli, P. D.; Agostiano, A. *J. Phys. Chem. B* **2005**, *109*, 1554.
- (81) Kavan, L.; Grätzel, M.; Gilbert, S. E.; Klemenz, C.; Scheel, H. J. *J. Am. Chem. Soc.* **1996**, *118*, 6716.
- (82) Micic, O. I.; Zhang, Y.; Cromack, K. R.; Trfunac, A. D.; Thurnauer, M. C. *J. Phys. Chem.* **1993**, *97*, 7277.
- (83) Fujishima, A.; Zhang, X.; Tryk, D. A. *Surf. Sci. Rep.* **2008**, *63*, 515.
- (84) Hossain, F. M.; Sheppard, L.; Nowotny, J.; Murch, G. E. *J. Phys. Chem. Solids* **2008**, *69*, 1820.
- (85) Umezawa, N.; Janotti, A.; Rinke, P.; Chikyow, T.; Van de Walle, C. G. *Appl. Phys. Lett.* **2008**, *92*, 041104.
- (86) Serpone, N.; Lawless, D.; Khairutdinov, R.; Pelizzetti, E. *J. Phys. Chem.* **1995**, *99*, 16655.
- (87) Lawless, D.; Serpone, N.; Meisel, D. *J. Phys. Chem.* **1991**, *95*, 5166.
- (88) Berger, T.; Sterrer, M.; Diwald, O.; Knözinger, E.; Panayotov, D.; Thompson, T. L.; Yates, J. T., Jr. *J. Phys. Chem. B* **2005**, *109*, 6061.
- (89) Howe, R. F.; Grätzel, M. *J. Phys. Chem.* **1987**, *91*, 3906.
- (90) Salvador, P. *J. Phys. Chem. C* **2007**, *111*, 17038.
- (91) Grätzel, M. *Nature* **2001**, *414*, 338.
- (92) Lyon, L. A.; Hupp, J. T. *J. Phys. Chem. B* **1999**, *103*, 4623.
- (93) Fabregat-Santiago, F.; Barea, E. M.; Bisquert, J.; Mor, G. K.; Shankar, K.; Crimes, C. A. *J. Am. Chem. Soc.* **2008**, *130*, 11312.
- (94) Mor, G. K.; Varghese, O. K.; Paulose, M.; Shankar, K.; Grimes, C. A. *Sol. Energy Mater. Sol. Cells* **2006**, *90*, 2011.
- (95) Paulose, M.; Varghese, O. K.; Mor, G. K.; Grimes, C. A.; Ong, K. G. *Nanotechnology* **2006**, *17*, 398.
- (96) Varghese, O. K.; Gong, D.; Paulose, M.; Ong, K. G.; Craig, C. A. *Sens. Actuators, B* **2003**, *93*, 338.

JP9090987